

Lamination of ultra-thin silicon wafers for producing high quality and low cost X-ray telescope mirrors

Youwei Yao* and Mark L. Schattenburg

Space Nanotechnology Lab, MIT Kavli Institute for Astrophysics and Space Research, Cambridge, MA, USA 02139

*yaoyw@mit.edu; phone: (847)868-6295; snl.mit.edu

ABSTRACT

We present a thin wafer lamination method for producing X-ray telescope mirrors aiming at $1\text{-}10''$ optics quality and low fabrication cost. Traditional grinding/polishing and hot slumping methods find difficulty to meet the required figure accuracy when the mirror thickness is below 1 mm. In this paper, we introduce a new fabrication procedure to satisfy those requirements: first, we laminate flat and ultra-thin silicon wafers on a well polished mandrel via direct bonding until the wafer stack achieves the designed thickness. Second, we release the stack from the mandrel since the direct bonding is temporary. Third, we anneal the stack to create permanent bonding and stabilize the deformation. In such a manner, the intrinsic waviness of each wafer can be alleviated. Our FEA simulation shows the RMS slope error of the stack surface released from a flat mandrel is improved by a factor of 6 when the layer number is doubled, regardless of the total thickness. In the case of a cylindrical mandrel, the local waviness could be improved by a factor of 4000, while a cone angle problem appears and needs to be resolved in future work. We also developed the fabrication method and successfully optimized our wafer cleaning process.

Keywords: X-ray optics, X-ray mirrors, Lamination, Ultra-thin silicon, Direct bonding

1. INTRODUCTION

Next generation X-ray telescopes require light weight optics with high angular resolution ($<1''$ for Lynx & $1\text{-}10''$ for a super-NuSTAR) and an effective area as large as Athena.^{1,2} Traditional mirror technologies such as the polishing and grinding method applied to produce Chandra's mirror would lead to an unaffordable fabrication cost.^{3,4} The hot slumping method is suitable for producing low cost glass mirrors with moderate optics quality,⁵ however, the potential ability of this method to provide arc-second optics still remains unknown.

Recently, silicon X-ray optics have been developed as a promising option for next generation X-ray telescopes. Based on development of the semiconductor industry, abundant techniques for silicon processing along with affordable mono-crystalline silicon material benefits X-ray optics. Sawing and polishing techniques applied to silicon bulk material has been used by the NASA Goddard Space Flight Center to produce high quality silicon mirror shells,^{6,7} while a direct bonding technique has been selected by Cosine to integrate silicon wafers for large-area silicon pore optic (SPO) mirrors for Athena.⁸

In our group, aiming at future low cost X-ray missions with $1\text{-}10''$ optic quality, a low cost ultrathin silicon lamination process is proposed. This process is based on the fact that the semiconductor industry can mass produce high surface quality (RMS roughness <1 nm) ultra-thin ($5\text{-}100\ \mu\text{m}$ @ 100 mm diameter) silicon wafers for reasonable cost. Figure 1 shows the sketch of the proposed process.

The idea is to laminate thin silicon wafers layer-by-layer on a polished Si mandrel or vacuum chuck by means of direct bonding, which is also similar to the optical contact bonding method. When the entire thickness reaches the desired value, the stack would be peeled off by inserting a thin blade between the first laminated layer and the mandrel. Since the silicon wafers are temporarily bonded with each other, the released stack would be annealed after the peeling step to create permanent bonds. The stack shape would deform after the peeling-off step until the residual stress of each layer reaches equilibrium. Our FEA model shows this spring-back effect is predictable, and therefore, the released stack shape is determined by the mandrel shape and the waviness of each individual wafer. The released stack would be used as an X-ray telescope mirror.

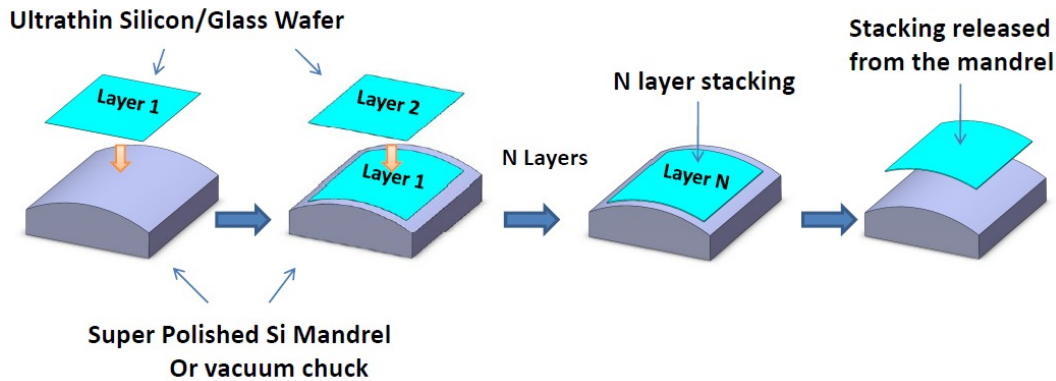


Figure 1. Sketch of lamination process

In this work, we established 2D and 3D FEA models in ABAQUS to demonstrate feasibility. A 2D model was used to simulate lamination on a flat mandrel. Three independent layer thicknesses including 25, 50 and 100 μm were used in the model to study the influence of layer thickness. An artificial sinusoidal waviness with 1 mm amplitude and random phase was added to each layer to demonstrate the surface improvement carried out by the lamination process. In the 3D model, a cylindrical mandrel has been presumed. The layer thickness is set to 50 μm and the number of layers is fixed at four to save calculation time.

A major challenge of the fabrication process has been dust contamination. The silicon wafer direct bonding/lamination process requires chemical treatment and surface activation of the wafers to achieve good bonding quality. Inadequate cleaning methods and lamination procedures could leave chemical residue and dust particle contamination on wafer surfaces, which could lead to problems such as delamination, voids and air pockets between the layers after stacking and thus reduce optics quality. Our current process uses an optimized chemical cleaning step. A commercial wafer bonding machine has been used to stack silicon wafers after cleaning. An infrared optics setup has been used to inspect the bonding quality. Since our current bonding result is repeatable and defect free, the conclusion has been made that our chemical cleaning process is successful. A new wafer lamination tool is under development to produce a mirror demonstrator in the future.

2. FEA SIMULATIONS

We built 2D and 3D FEA models using Schott D263T glass substrates to calculate the surface deformation of the released stack when intrinsic waviness exists in each individual layer. In these models, calculations are achieved by two steps. In Step 1, each layer in an N-layer stack is modeled individually without interaction. These layers with initial waviness are deformed into the mandrel shape and the stress distribution of the layers are calculated sequentially. In Step 2, the calculated stress distribution is propagated into the N-layer stacking model in which the layer surfaces are bonded with each other. In this step, the N-layer stacking has a perfect initial surface shape (mandrel shape). The surface deformation after release is calculated based on the stress relaxation of each layer.

2.1 2D FEA Simulation

The 2D model simulates the simplest situation of a mandrel. In this case we only consider the cross section of mirrors and mandrels. In this simulation substrates of diameter 200 mm and three thicknesses of 25, 50 and 100 μm are set in independent models to study the influence of layer thickness. Each individual layer has an initial sinusoidal waviness of 1 mm amplitude and 200 mm period on the surface, producing 4000" initial RMS slope error. The phase of the waviness is randomized as is shown in Figure 2.

In the simulation, the stress calculation in Step 1 is reversed to simplify the meshing process, which is demonstrated as follows. The initial glass layers are assumed to have perfectly flat surfaces. The target deformation is set to a sinusoidal function. The calculated stress distribution is multiplied with a negative sign to inverse the simulated deformation, i.e., deforming from sinusoidal shape to perfectly flat.

In the 2D models, all layers are meshed to 10000 rectangular elements (25 layers by 400 columns). The type of the meshed element is set to CPS4I in ABAQUS, which is an incompatible mode plane stress element which treats the cross section as a beam.

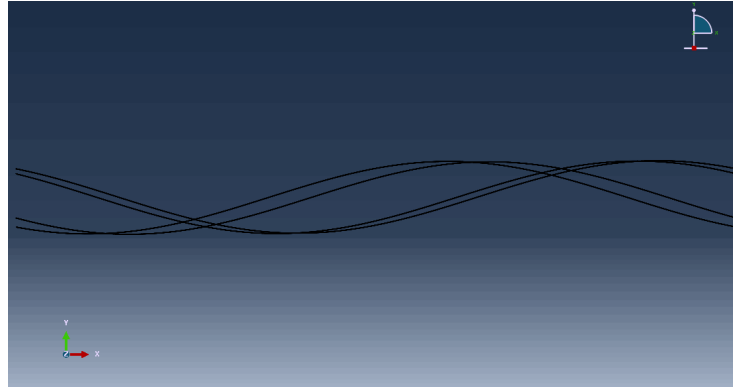


Figure 2. Example of an artificial initial waviness generated on four glass layers. Glass layers have no interaction. Glass dimension is 200 mm diameter by 100 μm thickness. Each layer has 1 mm amplitude sinusoidal waviness with random phase.

When the calculated stress is propagated into an N-layer stacking model from a flat initial surface, the deformed surface profile is calculated in Step 2. Since Step 1 is a random process, 1000 iterations between Step 1 and Step 2 are performed for a fixed number of layers. Figures 3 and 4 show examples of calculation results.

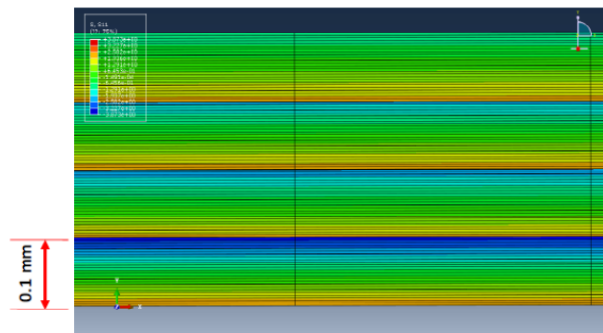


Figure 3. Residual stress distribution of S_{xx} in a four layer stack calculated in Step 2. Note: stack is partially plotted due to high aspect ratio. Dimension of the plot area is 1 mm by 0.4 mm. Solid lines represent the rectangular mesh. Stress varies from -3.87 MPa to 3.87 MPa (from red to blue)

Figure 5 shows the calculated RMS slope error for the number of layers varying from 1 to 16. Different colors represent 2D models using different layer thicknesses. The error bar on each data point is produced by 1000 iterations of random waviness.

Based on the 2D results shown in Figure 5, when the initial slope error of each individual layer is fixed at $4000''$, doubling the number of layers improves the surface by a factor of ~ 6 . The three colors of lines are overlapped with each other, indicating the surface improvement resulting from the lamination process is thickness independent.

A 2D simulation of stacking layers on a flat mandrel is useful to validate prototype fabrication process in the near future. From a practical point of view, a 3D simulation using a cylindrical shape is important to help develop a telescope mirror shell stacking process in the long term.

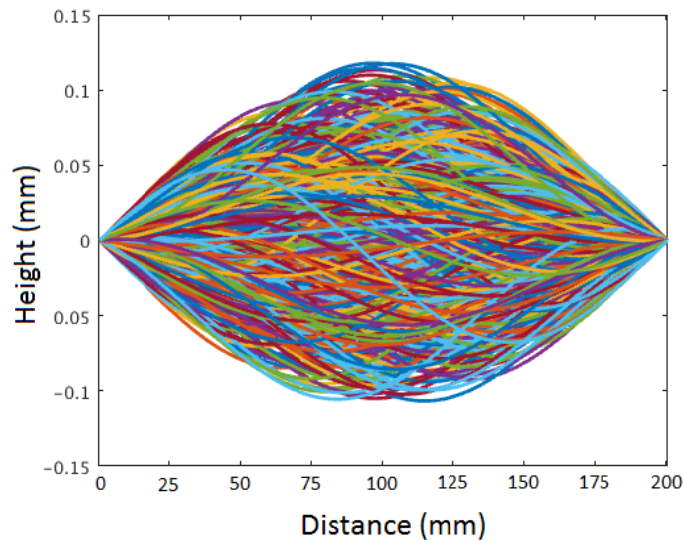


Figure 4. Surface profiles of a four-layer stack calculated in Step 2 after 1000 iterations. Thickness of each layer is 0.1 mm. Profiles are leveled by the tips of the lines.

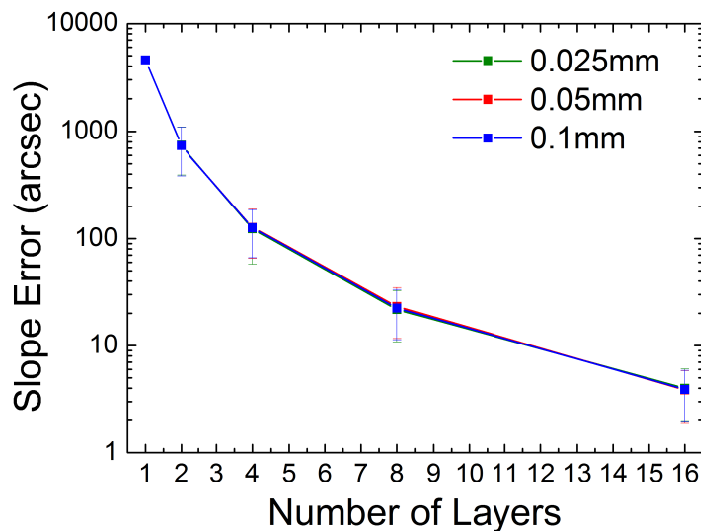


Figure 5. Calculated RMS slope error of a 2D stack.

2.2 3D FEA Simulation

Since 3D simulation is time consuming, in this preliminary study, the number of layers is fixed at four and the thickness of glass layers is fixed at 50 μm . The dimension of glass pieces is set at 200 mm long by 100 mm wide which is close to NuSTAR's mirror size. We assume the mandrel is a 100 mm radius cylinder, which means the initial surface of the four-layer stack is a cylindrical shape with the same radius of curvature along the azimuthal direction. In this simulation, all layers are meshed to 12500 cuboidal elements (50 rows by 100 columns by 25 layers). The element type is selected as C3D8I in ABAQUS software which is standard for 3D stress and strain.

During 3D simulation, we used the same two-step process as has been introduced in 2D case. In addition, we used two different simulations for different purposes. In Simulation #1, the goal is to determine the shape of a stack released from a cylindrical mandrel. Therefore, four layers are presumed to have initially a perfect flat surface. In Simulation #2,

the purpose is to investigate the influence of individual layer's initial shape. Thus, artificial sinusoidal waviness is assumed on each layer along the direction of X-ray reflection.

2.2.1 Simulation #1

The initial shape of individual layers is assumed perfectly flat. In Step 1, each independent layer is deformed into a cylindrical shape. The stress distribution is calculated. In Step 2, a four-layer cylindrical stack which has a 100 mm surface radius is established in a model. Stress calculated in Step 1 is propagated into the corresponding layers to create deformation. After deformation, profiles along Lines 1 to 4 as shown in Fig. 6 are plotted in Figs. 7 and 8.

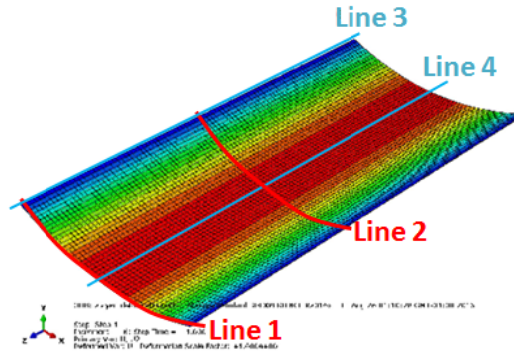


Figure 6. Sketch of the lines on a four-layer stack to be plotted

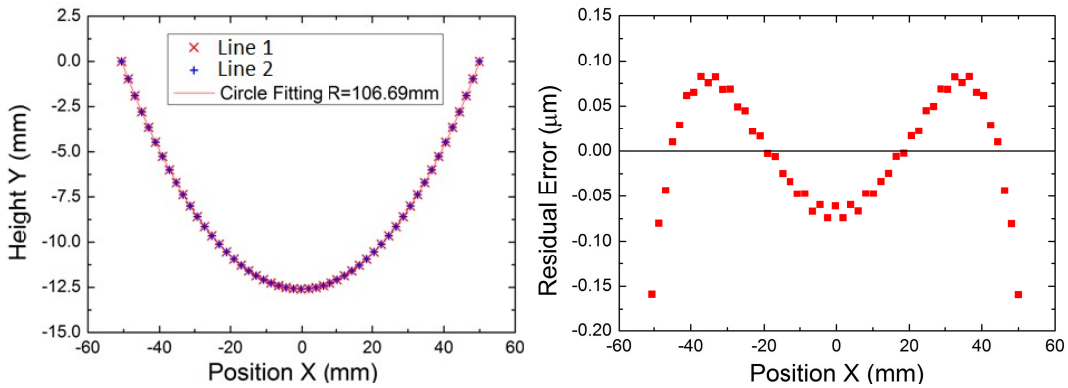


Figure 7. Left: Calculated surface profile along Lines 1 and 2 shown in Figure 6, and a fitted result. Right: Residual between Line 2 and its fitting line.

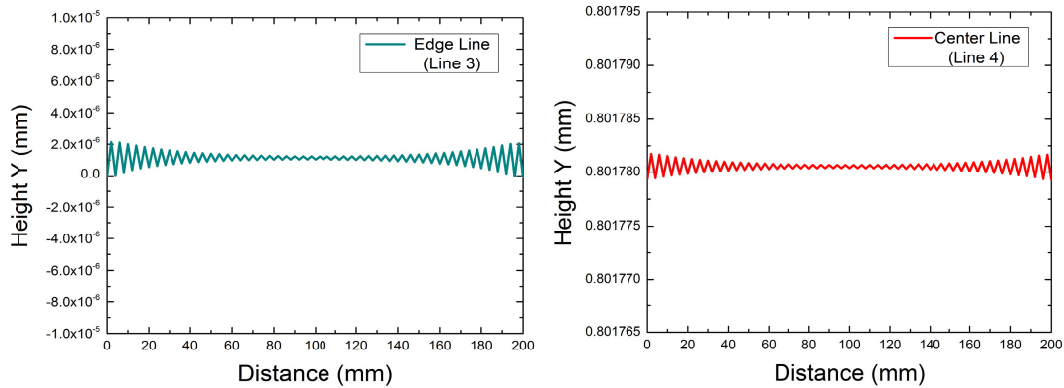


Figure 8. Calculated profile along Line 3 (left) and Line 4 (right)

In Figure 7, the left panel shows the calculated profiles along Lines 1 and 2. The solid line is the result of a curve fit to Line 2, which is represented by a circle function. The fitted radius of curvature is 106.69 mm which is 6.69 mm larger than the initial value. This indicates the stack as released from a cylindrical mandrel springs back due to residual stress. The right panel shows the residual between Line 2 and its fitted result. The $\sim 0.15 \mu\text{m}$ residual along the azimuthal direction should be negligible.

In Figure 8, the nanometer level oscillation is presumably due to numerical artifacts, indicating Lines 3 and 4 are straight after stacking.

Based on the results shown above, the stack released from a cylindrical surface springs back radially, however, the deformed surface is still cylindrical.

2.2.2 Simulation #2

In this simulation, sinusoidal waviness was added on individual layers along the long direction in Step 1, as is shown in Figure 9. The amplitude of the waviness is 1 mm and the period is 200 mm. Waviness phase was randomized. In this simulation, stresses of each layer are created by two factors. The first one is the stress created by flattening the initial waviness during the lamination. Similar as Step 1 in the 2D simulation, this is calculated by deforming flat glass pieces into designed profiles and then inverting the sign. The second factor is the stress generated by bending the flat mirror into a cylindrical shape, which is the stress calculated in Simulation #1. In this model, we preliminarily assume stresses created by deformation along orthogonal directions on a flat piece are still orthogonal. Therefore, the stresses calculated from the artificial waviness are added with stresses from Simulation #1 to simulate the total stress created during lamination. In Step 2, the sum of the stresses are propagated into the cylindrical stack model. Calculated profiles along Line 4 (center line) are plotted for randomized phase, as shown in Figure 10.

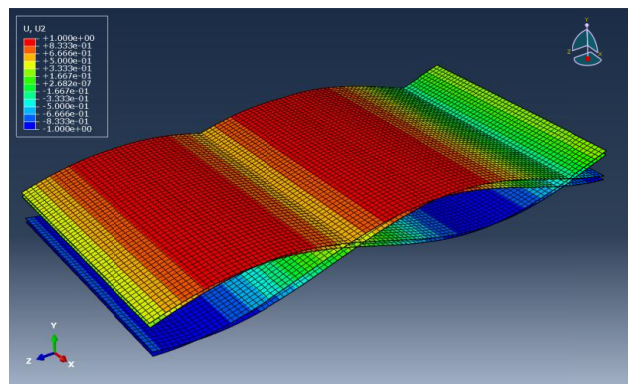


Figure 9. Example of an artificial sinusoidal waviness generated along the z direction on four glass layers. Glass layers have no interaction. Glass dimension is 200 mm by 100 mm by 50 μm . Each layer has a 1 mm amplitude sinusoidal waviness with random phase.

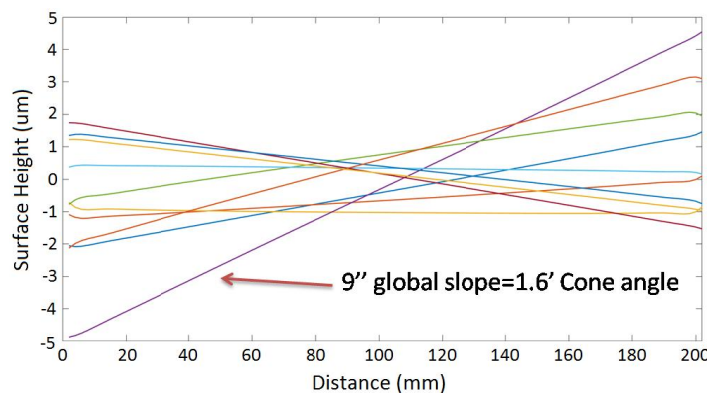


Figure 10. Calculated surface profiles along Line 4 (center line) in Figure 6. Each line represents a calculation result with a specific phase distribution.

Since Simulation #2 includes random waviness in each layer, 10 iterations through Step 1 and Step 2 are made to explore a range of possibilities. As is shown in Figure 10, a global slope error is observed on each line which could be explained by the boundary conditions in the 3D model, as is shown in Figure 11. The cylindrical stack is constrained by three corners: Corner A is totally constrained, Corner B can slide along the X direction and corner C can slide along the X and the Y direction. Thus, the corners are constrained within a fixed plane. The global slope error could be created by a cone angle due to the random waviness of each individual glass layer. For example, the purple line in Figure 10 has the highest global slope error which is about 9". Calculation results show the corresponding cone angle is 1.6', which is fairly large for arc-second optics. However, the 1 mm amplitude waviness assumption is probably much higher than the real case. In addition, some efforts such as clocking the wafers before lamination could be effective to balance or reduce the cone angle. Further analysis is needed to help understand this issue.

If the global slope error is removed from the lines in Figure 10 by subtracting a linear fit, then the local RMS slope error is within the 1" level as shown in Figure 12, which is much better than hot slumping results. Therefore, a conclusion has been made that in the 3D case, a four-layer stack could significantly reduce the local slope error on each individual layer by a factor of ~4000.

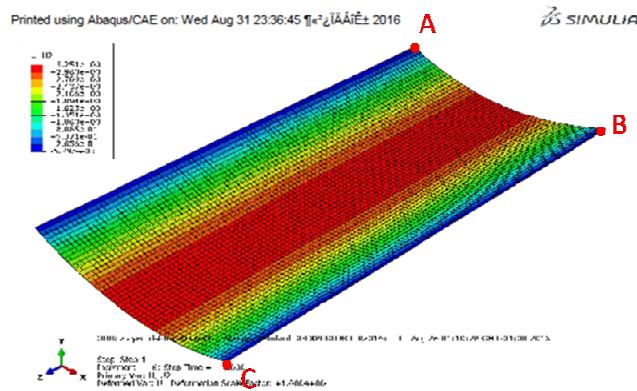


Figure 11. Demonstration of boundary conditions in the 3D simulation.

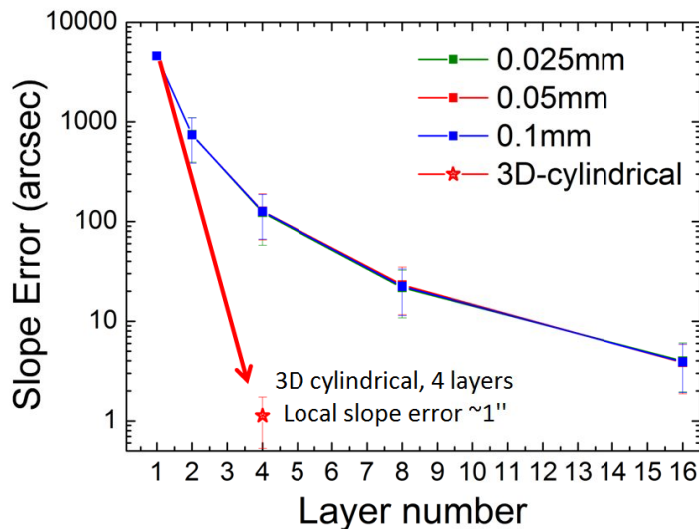


Figure 12. Comparison between 2D and 3D four layer stacking results

3. FABRICATION PROGRESS

Since the lamination process requires a direct bonding method, we have recently focused on bonding silicon wafers due to their excellent surface quality and low RMS slope error. We selected some regular commercial wafers and measured the surfaces using a Shack-Hartmann metrology tool, with typical RMS slope errors of 500 μm -thick Si wafers around 25", while for 200 μm thick wafers this value increased to 60". We believe the RMS slope error of ultra-thin silicon wafers such as 80 μm thickness could be much lower than the set value in our FEA simulation which is 4000".

For the direct bonding technique, four critical points need to be satisfied. First, the bonding surfaces need to be ultra-smooth which means the RMS roughness should be below 1 nm. Second, surfaces need to be ultra-clean, i.e., free of dust particles and chemical contamination. Third, appropriate contacting force is necessary for the bonding. Fourth, temporarily bonded wafers need to be annealed to improve bonding strength. Points 1, 3 and 4 are easy to be realized. However, the requirement of ultra-clean surface is determined by the cleaning and lamination process which needs to be optimized. In our current experiment, we optimized the chemical cleaning process. We find a 1 μm thick thermal oxide growth followed by BOE oxide strip and piranha cleaning is the most effective. The chemically cleaned wafers are bonded using a commercial wafer bonding machine EV620 as is shown in Figures 13a and 13b. The bonded wafers are inspected by an infrared optics system (see Figure 13c) thus the bonding quality could be confirmed.

Figure 13c shows the infrared inspection system in our lab. Since silicon wafers are infrared transparent, local separation between stacked layers creates Newton rings in the transmission image. Thus, dust particles, air pockets and delamination are visible in this system as long as the delamination gap is larger than a quarter of the infrared wavelength which is about 300 nm. Figure 14 shows infrared images of bonded wafer pairs. All wafers shown are 100 mm in diameter and 400 μm thick.

As is shown in the Figure 14 (left), dust particles, voids and delamination exist between bonded wafer pairs due to inadequate wafer cleaning. There are no features when the process is optimized, as is shown in the right picture which indicates high bonding quality.

We also bonded three wafers by using the same process. The infrared image of this three-layer stack is shown in Figure 15. The excellent bonding result indicates that the stacking of ultra-thin silicon wafers on a flat mandrel is possible. We are planning to integrate an ultra-flat vacuum pin chuck into the bonding machine and then stack four layers to produce a flat demonstrator. We are also planning to build an ultra-thin wafer lamination system for a cylindrical mandrel.

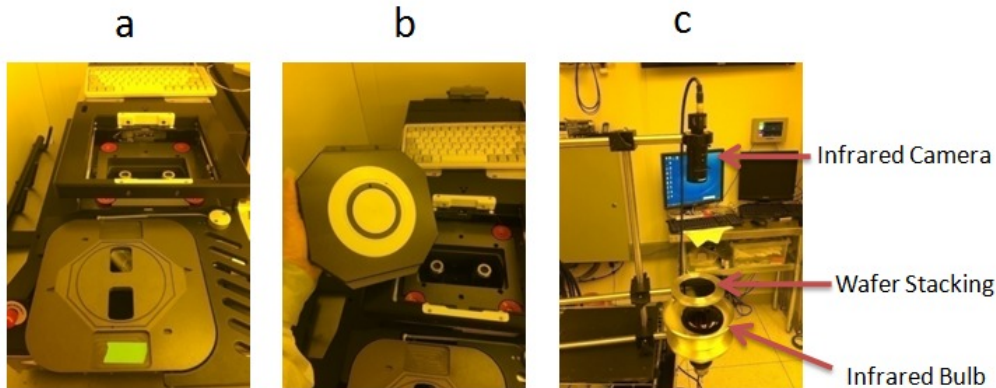


Figure 13. a and b show a commercial wafer bonding machine EV620: a is the bottom wafer chuck, b is the top wafer chuck with a piston at center and c is the infrared test setup for inspecting wafer bonding quality.

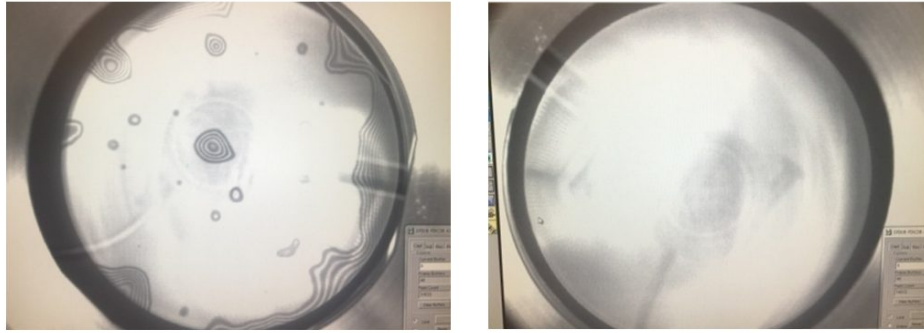


Figure 14. Comparison between the bonding results before (left) and after (right) optimizing the chemical cleaning process.

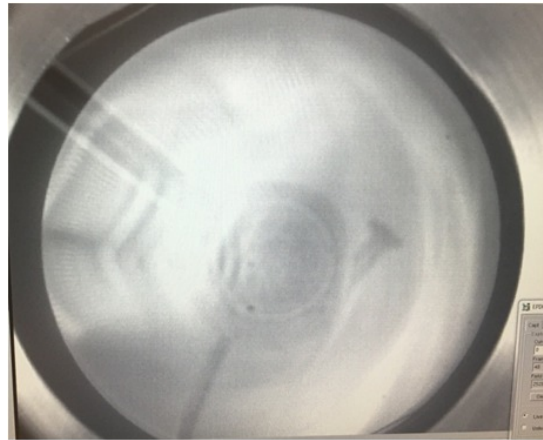


Figure 15. Infrared transmission image of a three-layer stack.
Note: patterns on the wafer are due to the reflection from the infrared camera.

4. CONCLUSIONS

We demonstrated an ultra-thin Si wafer lamination method to fabricate low cost X-ray telescope mirrors with 1-10" level optics quality. 2D FEA simulations using a flat mandrel showed that doubling the number of layers improves the surface RMS slope error of the stack surface by a factor of ~ 6 , regardless of the layer thickness. 3D FEA simulations demonstrated that for a cylindrical mandrel with $R=100$ mm, a four-layer lamination improves the local RMS slope error by a factor of ~ 4000 , but with a cone angle error which might be resolved in future work. For the fabrication progress, a wafer cleaning process has been successfully optimized. High quality and repeatable Si wafer direct bonding results were achieved by a commercial bonding machine EV620. We plan to integrate an ultra-flat vacuum pin chuck into the bonding machine to produce a flat four-layer Si wafer stack as a demonstrator in the near future.

ACKNOWLEDGMENTS

This work was supported in part by NASA APRA funding. The authors would like to thank William W. Zhang of the NASA Goddard Space Flight Center, Lester Cohen of Harvard-SAO, and Brandon Chalifoux and Ralf Heilmann for advice.

REFERENCES

- [1] M. C. Weisskopf, J. Gaskin, H. Tananbaum, A. Vikhlinin, "Beyond Chandra – the X-ray Surveyor," arXiv: 1505.00814 (2015)

- [2] S. L. O'Dell, R. Allured, A. O. Ames, M. P. Biskach, D. M. Broadway, R. J. Bruni, D. N. Burrows, J. Cao, B. D. Chalifoux, K. W. Chan, Y. W. Chung, V. Cotroneo, R. F. Elsner, J. A. Gaskin, M. V. Gubarev, R. K. Heilmann, E. Hertz, T. N. Jackson, K. Kilaru, J. J. Kolodziejczak, R. S. McClelland, B. D. Ramsey, P. B. Reid, R. E. Riveros, J. M. Roche, S. E. Romaine, T. T. Saha, M. L. Schattenburg, D. A. Schwartz, E. D. Schwartz, P. M. Solly, S. Troler-Mckinstry, M. P. Ulmer, A. Vikhlinin, M. L. Wallace, X. Wang, D. L. Windt, Y. Yao, S. Ye, W. W. Zhang and H. Zuo, "Toward large-area sub-arcsecond X-ray telescopes II", Proc. SPIE 9965, 996507 (2016)
- [3] M. C. Weisskopf, H. D. Tananbaum, L. P. Van Speybroeck and S. L. O'Dell, "Chandra X-ray observatory (CXO): Overview," Proc. SPIE 4012, 2-16 (2000).
- [4] D. A. Schwartz, L. P. David, R. H. Donnelly, R. J. Edgar, T. J. Gaetz, D. E. Graessle, D. Jerius, M. Juda, E. M. Kellogg, B. R. McNamara, P. P. Plucinsky, L. P. Van Speybroeck, B. J. Wargelin, S. Wolk, P. Zhao, D. Dewey, H. L. Marshall, N. S. Schulz, R. F. Elsner, J. J. Kolodziejczak, S. L. O'Dell, D. A. Sartz, A. F. Tennant, and M. C. Weisskopf, "Absolute effective area of the Chandra high-resolution mirror assembly (HRMA)," Proc. SPIE 4012, 28-40 (2000).
- [5] W. W. Zhang, "Manufacture of Mirror Glass Substrates for The NUSTAR Mission," Proc. SPIE 7437, 74370N-1 (2009).
- [6] W. W. Zhang, "Lightweight and high-resolution single crystal silicon optics for X-ray astronomy," Proc. SPIE 9905, 99051S (2016).
- [7] R. E. Riveros, M. P. Biskach, K. D. Allgood, J. R. Mazzeola, M. V. Sharpe and W. W. Zhang, "Progress on the fabrication of high resolution and lightweight monocrytalline silicon X-ray mirrors," Proc. SPIE 9905, 990521 (2016).
- [8] M. Bavdaz, E. Wille, B. Shortt, S. Franssen, M. Collon, N. Barriere, A. Yanson, G. Vacanti, J. Haneveld, C. van Baren, K. Zuknik, F. Christensen, D. D. M. Ferreira, M. Krumrey, V. Burwitz, G. Pareschi, D. Spiga, G. Valsecchi and D. Vernani, "The ATHENA optics development," Proc. SPIE 9905, 990527 (2016)